

This discussion paper is/has been under review for the journal Atmospheric Chemistry and Physics (ACP). Please refer to the corresponding final paper in ACP if available.

Effect of gravity wave temperature fluctuations on homogeneous ice nucleation in the tropical tropopause layer

T. Dinh¹, A. Podglajen², A. Hertzog², B. Legras³, and R. Plougonven²

¹Program in Atmospheric and Oceanic Sciences, Princeton University, Princeton, New Jersey, USA

²Laboratoire de Météorologie Dynamique, École Polytechnique, Palaiseau, France

³Laboratoire de Météorologie Dynamique, École Normale Supérieure, Paris, France

Received: 3 March 2015 – Accepted: 8 March 2015 – Published: 24 March 2015

Correspondence to: T. Dinh (tdinh@princeton.edu)

Published by Copernicus Publications on behalf of the European Geosciences Union.

8771

Abstract

The impact of high-frequency fluctuations of temperature on homogeneous nucleation of ice crystals in the vicinity of the tropical tropopause is investigated using a bin microphysics scheme for air parcels. The imposed temperature fluctuations come from measurements during isopycnic balloon flights near the tropical tropopause. The balloons collected data at high frequency, guaranteeing that gravity wave signals are well resolved.

With the observed temperature time series, the numerical simulations with homogeneous freezing show a full range of ice number concentration (INC) as previously observed in the tropical upper troposphere. In particular, low INC may be obtained if the gravity wave perturbations produce a non-persistent cooling rate (even with large magnitude) such that the absolute change in temperature remains small during nucleation. This result is explained analytically by a dependence of the INC on the absolute drop in temperature (and not on the cooling rate). This work suggests that homogeneous ice nucleation is *not* necessarily inconsistent with observations of low INC.

1 Introduction

Cirrus clouds have an important impact on the global radiative energy budget (Lohmann and Roeckner, 1995). In the tropical tropopause layer (TTL, Fueglistaler et al., 2009), cirrus clouds contribute to the radiative heating (Corti et al., 2006; Dinh and Fueglistaler, 2014a) and control the dehydration of the air before entry into the stratosphere (Brewer, 1949; Jensen et al., 1996; Dinh and Fueglistaler, 2014b). For all cirrus clouds, the radiative and climate impact, ability to modify water vapour, and cloud evolution are sensitive to the ice number concentration (e.g. Kärcher et al., 2014), which depends strongly on the nucleation process of ice crystals.

When evaluating the ice number concentration (INC) produced by nucleation, it has been often assumed that the relevant time scale is sufficiently short such that the verti-

8772

cal velocity and associated adiabatic cooling rate remain constant (e.g. Barahona and Nenes, 2008). For constant cooling rate, homogeneous freezing of aqueous aerosols produces higher INC ($> 1000 \text{ L}^{-1}$) than those commonly observed ($< 100 \text{ L}^{-1}$) in cirrus clouds (Lawson et al., 2008; Krämer et al., 2009; Davis et al., 2010). Observations and calculations of INC based on homogeneous freezing can be reconciled only if very low vertical speeds ($w < 0.01 \text{ m s}^{-1}$) are used in the simulations. This seems at odds with the ubiquitous presence of atmospheric gravity waves, which typically generate an order of magnitude larger disturbances in the vertical velocity. Therefore, it has been suggested that heterogeneous freezing (instead of homogeneous freezing) is the dominant nucleation mechanism for cirrus clouds in the upper troposphere (Jensen et al., 2010, 2012). The INC obtained by heterogeneous freezing is apparently limited by the availability of suitable ice nuclei (generally less than 100 L^{-1}) in the upper troposphere (Chen et al., 1998; Rogers et al., 1998).

However, Spichtinger and Krämer (2013) pointed out that high-frequency variations in temperature and cooling rates can substantially decrease the INC produced during homogeneous nucleation compared to those obtained with constant updraft speeds. Yet, their numerical results are based on ideally constructed temperature time series, and so remain somewhat conceptual. The present work complements their study by using temperature time series data collected at high temporal resolution during long-duration balloon flights near the tropical tropopause. The observed temperatures contain perturbations from a spectrum of atmospheric waves, with periods ranging from days to minutes. Our analysis of the nucleation simulations based on these observed time series confirms the earlier results of Spichtinger and Krämer (2013), and furthermore reveals an exponential relationship between the INC and the absolute change in temperature during the nucleation events.

The article is organised as follows. Sections 2 and 3 describe the balloon data and the technical details of the model used here to simulate homogeneous ice nucleation. Section 4 presents the numerical results. Section 5 provides the theoretical basis ex-

8773

plaining how the fluctuations in time of temperature may affect homogeneous ice nucleation. Section 6 contains the conclusions.

2 Balloon data descriptions

The temperature time series used in this study are derived from data collected by two long-duration, superpressure balloons launched by the French Space Agency from Seychelles Islands (55.5° E , 4.6° N) in February 2010 in the framework of the Pre-Concordiasi campaign (Rabier et al., 2010). The balloons flew at an altitude of about 19 km, and achieved circumterrestrial flights, therefore sampling the whole equatorial area. Details on the balloon trajectories and large-scale atmospheric dynamics during the flights can be found in Podglajen et al. (2014). Superpressure balloons are advected by the wind on isopycnic (constant-density) surfaces and therefore behave as quasi-Lagrangian tracers of atmospheric motions. A further remarkable property of superpressure balloons is their sensitivity to atmospheric gravity waves (Massman, 1978; Nastrom, 1980; Boccara et al., 2008; Vincent and Hertzog, 2014). The sampling frequency of the balloon position, atmospheric pressure and temperature during the campaign is every 30 s.

Here, we do not use the temperature observations gathered during the flights to constrain the nucleation simulations; these time series tend to be both too noisy and warm biased during daytime. Instead, we infer the temperature disturbances from the balloon vertical displacements (ζ'_b), which are obtained by band-pass filtering the raw GPS altitudes to exclude planetary-wave motions (low cut-off frequency $f_{\text{low}} = (24 \text{ h})^{-1}$) and balloon own motions (high cut-off frequency $f_{\text{high}} = (10 \text{ min})^{-1}$). The high cut-off frequency is sufficiently large to enable us to resolve almost the full spectrum of gravity waves, which extends up to the Brunt–Väisälä frequency ($\sim (4 \text{ min})^{-1}$) in the equatorial lower stratosphere and $\sim (10 \text{ min})^{-1}$ in the TTL). The isentropic air parcel vertical

8774

4 Numerical simulations

For adiabatic motions, the effect of pressure variations on the water vapour mixing ratio (r) can be neglected compared with that due to temperature variations. Assuming constant air pressure, we prescribe an initial water vapour content for the air parcels
 5 such that nucleation occurs at a chosen temperature T_0 . This is possible because the saturation ratio at the threshold of nucleation S_{nuc} is a function of temperature (Koop et al., 2000; Kärcher and Lohmann, 2002; Ren and Mackenzie, 2005), and it is related to the initial water vapour mixing ratio of air parcels by

$$r_0 = \frac{e_{\text{sat}}(T_0) S_{\text{nuc}}(T_0) R_a}{\rho R_v}, \quad (4)$$

10 where e_{sat} is the saturation water vapour pressure, and R_a and R_v are respectively the gas constants of air and water vapour. The notations $e_{\text{sat}}(T_0)$ and $S_{\text{nuc}}(T_0) \equiv S_0$ refer to respectively e_{sat} and S_{nuc} at T_0 . Note that, up to the nucleation time the vapour mixing ratio r is conserved. As illustrated in Fig. 1, every air parcel follows an isoline of constant water vapour mixing ratio ($r = r_0$) until crossing the $S_{\text{nuc}}(T)$ curve, at which
 15 point nucleation begins.

The simulations were first carried out for pressure $p = 100$ hPa, nucleation temperature $T_0 = 195$ K, and deposition coefficient $\alpha = 0.05$ (Sects. 4.1, 4.2, and 4.3.1). A nucleation event is defined to start when the rate of nucleation exceeds a threshold J_ε , and to end when it becomes less than J_ε . For our simulations, choosing a threshold
 20 of $J_\varepsilon = 1 \text{ L}^{-1} \text{ s}^{-1}$, we have $S_0 = 1.509$ for $T_0 = 195$ K. Sensitivities to T_0 in the range between 180 and 210 K, and α in the range between 0.001 and 1 are discussed in Sects. 4.3.2 and 4.3.3. Time series of temperature is defined by

$$T(t) = T_0 + T'(t), \quad (5)$$

where $T'(t)$ are either idealised following temperature variations associated with constant and time-varying vertical velocities (Sects. 4.1 and 4.2), or taken from the balloon
 25 data (Sect. 4.3).

8777

4.1 Constant vertical velocity

Here temperature is set to decrease with time due to adiabatic cooling at a constant vertical velocity in a hydrostatic background, i.e.

$$T'(t) = -\frac{g}{c_p} w t. \quad (6)$$

5 We simulated five nucleation events with $w = 10^k \text{ ms}^{-1}$, where $k = \{-3, \dots, 1\}$.

As shown in Fig. 2 (blue circles), for $w < 1 \text{ ms}^{-1}$ the number of ice crystals nucleated N_i increases with w . For $w \geq 1 \text{ ms}^{-1}$, all aerosols particles form ice, hence $N_i = N_a = 200 \text{ cm}^{-3}$. Figure 2 shows that if the vertical velocity and the cooling rate are constant during the nucleation events, w must be less than 0.01 ms^{-1} in order that
 10 $N_i \leq 100 \text{ L}^{-1}$. This result is consistent with previous studies (e.g. Krämer et al., 2009) of homogeneous freezing under constant vertical velocity.

4.2 Nonpersistent cooling

Here we vary w with time so that the rate of change of temperature $\frac{dT}{dt}$ is no longer constant with time. Specifically, we set

$$15 \quad w(t) = \begin{cases} +0.02 \text{ ms}^{-1} & \text{if } t \leq t_s, \\ -0.02 \text{ ms}^{-1} & \text{if } t > t_s. \end{cases} \quad (7)$$

The time t_s at which w and hence $\frac{dT}{dt}$ switch signs is varied by setting $t_s = \{20; 24; 28; 32; 36\}$ min. Figure 3 shows the evolution of temperature, saturation ratio and INC during the five nucleation events forced by $w = \pm 0.02 \text{ ms}^{-1}$ as defined above.

10 In the two events where w switches signs at 32 and 36 min (blue curves in Fig. 3), the maximum saturation ratio (S_{max}) is obtained at $t = t^*$ (31 min) before the minimum temperature (T_{min}) is reached. The saturation ratio decreases after t^* because water

8778

4.3.2 Sensitivity of INC to nucleation temperature

Here, we prescribe the initial vapour content r_0 of the air parcels such that the nucleation temperature is either $T_0 = 180$ or 210 K. In Fig. 1, this is equivalent to choosing another isoline of r and displacing accordingly the values of T_0 and S_0 at nucleation. As in the previous section, the balloon temperature perturbations are added to these nucleation temperatures to obtain the temperature time series $T(t)$, see Eq. (5).

The number of ice crystals nucleated for $T_0 = 180$ and 210 K is shown in Fig. 6. The data for $T_0 = 195$ K shown previously in Fig. 5 generally lie between the data points for $T_0 = 180$ and 210 K, that is, there is a monotonic relationship between N_i and T_0 . For the same ΔS , N_i is smaller for smaller T_0 . Conversely, for the same ΔT , N_i is smaller for larger T_0 .

4.3.3 Sensitivity of INC to deposition coefficient

The number of ice crystals nucleated at $T_0 = 195$ K for $\alpha = 0.001$ and $\alpha = 1$ is shown in Fig. 7. Notice that the transition from temperature-limit events to vapour-limit events occur at lower INC for $\alpha = 1$ than $\alpha = 0.001$. This makes sense because the ice crystals deplete water vapour at a faster rate in the case $\alpha = 1$, and so the number of ice crystals needed to significantly deplete water vapour is smaller.

For temperature-limit events, the functional dependence of N_i on ΔS (or ΔT) is invariant for different values of α , i.e. N_i is independent of α . However, for vapour-limit events, N_i is smaller for $\alpha = 1$ than $\alpha = 0.001$ for the same ΔS (or ΔT). The sensitivity of vapour-limit events to the deposition coefficient is explained in the theory section below.

5 Theory and discussions

In this section we provide the theoretical basis that explains the numerical results shown previously in Sect. 4.

8781

5.1 Formula for ice number concentration

The rate of nucleation of ice crystals during a nucleation event is given by

$$\frac{dN}{dt} = (N_a - N)JV_a, \quad (10)$$

where N_a is the aerosol particle number concentration, V_a is the volume of each aerosol particle, and J is the homogeneous nucleation rate given by Koop et al. (2000, their Eq. 7). By integrating Eq. (10) from the beginning ($t = t_0$) to end ($t = t_0 + \tau$) of the nucleation event we obtain

$$\ln\left(1 - \frac{N_i}{N_a}\right) = -V_a \int_{t_0}^{t_0+\tau} J dt = -V_a J_{\max} \int_{t_0}^{t_0+\tau} \exp(\ln(J) - \ln(J_{\max})) dt, \quad (11)$$

where $J_{\max} \equiv J(t^*)$ is the maximum value of J during the nucleation event ($t_0 < t^* < t_0 + \tau$), and $N_i \equiv N(t_0 + \tau)$ is the INC obtained at the end of the nucleation event. Following the steepest descent method, we obtain

$$\ln\left(1 - \frac{N_i}{N_a}\right) \approx -V_a J_{\max} \int_{t_0}^{t_0+\tau} \exp\left(\frac{1}{2} \frac{d^2(\ln J)}{dt^2}(t^*)(t - t^*)^2\right) dt, \quad (12)$$

$$\ln\left(1 - \frac{N_i}{N_a}\right) \approx -V_a J_{\max} \int_{t_0-t^*}^{t_0+\tau-t^*} \exp(-\mu^2 t^2) dt \approx -V_a J_{\max} \int_{-\infty}^{\infty} \exp(-\mu^2 t^2) dt, \quad (13)$$

$$\ln\left(1 - \frac{N_i}{N_a}\right) \approx \sqrt{\pi} V_a \frac{J_{\max}}{\mu}, \quad (14)$$

where

$$\mu^2 = -\frac{1}{2} \frac{d^2(\ln J)}{dt^2}(t^*) = -\frac{1}{2J_{\max}} \frac{d^2 J}{dt^2}(t^*). \quad (15)$$

8782

temperature-limit events. For vapour-limit events, Eq. (20) overestimates N_i because it neglects the depletion of water vapour during the nucleation events.

For $\alpha = 0.001$ and $\alpha = 1$, the INC obtained for $T_0 = 195$ K is shown in Fig. 7. Equations (16)–(20) predict that the relationship between N_i and ΔS for all events, and the relationship between N_i and ΔT for temperature-limit events do not change with the deposition coefficient. These theoretical predictions are shown by the solid curves in Fig. 7 obtained with constant $\mu = 0.02 \text{ s}^{-1}$. For $\alpha = 1$, the theoretical curve overestimates N_i for vapour-limit events that produce more than 10^3 L^{-1} ice crystals (Fig. 7a). We attribute this error to the assumption that μ is constant over the shown range of ΔS . In fact, the deposition coefficient governs the growth rate of ice crystals and affects how the saturation ratio changes with time, and how μ changes with ΔS (a consequence of Eq. 19). Our calculations indicate that the partial derivative of μ with respect to ΔS increases with α . For high values of α , calculation of N_i (especially for vapour-limit events) must account for the variations in μ as ΔS varies.

5.3 Dependence of INC on the initial water vapour mixing ratio

The temperature time series $T(t)$ along the trajectory of an air parcel (recall Eq. 5) and the initial water vapour content r_0 of the parcel are two independent conditions to be specified for the simulations. The initial water vapour content r_0 has a one-to-one relationship with the temperature at the threshold of nucleation T_0 via Eq. (4). In Sect. 4 we have studied how the INC varies with the various forms of $T(t)$ for a given r_0 and a corresponding T_0 . Here, on the other hand, we discuss how the INC varies as r_0 and T_0 vary for a given $T(t)$.

Now, consider air parcels with slightly different initial water vapour mixing ratios, r_0 and $r_0 + \delta r_0$. The nucleation temperatures for these air parcels are respectively T_0 and $T_0 + \delta T_0$ (see illustration in Figs. 1 and 8). For constant pressure, δr_0 and δT_0 are related

8785

by

$$\frac{\delta r_0}{r_0} = \frac{\delta e_{\text{sat}}}{e_{\text{sat}}} + \frac{1}{S_0} \frac{dS_0}{dT_0} \delta T_0 = \frac{L_s}{R_v T_0^2} \delta T_0 + \frac{1}{S_0} \frac{dS_0}{dT_0} \delta T_0 \quad (21)$$

by Eq. (4) and the Clausius–Clapeyron relation. The first term dominates the right hand side of Eq. (21), from which we obtain

$$\frac{dT_0}{dr_0} \approx \frac{R_v T_0^2}{L_s r_0}, \quad (22)$$

which indicates that T_0 increases monotonically with r_0 . For a given temperature time series $T(t)$, the minimum temperature T_{min} experienced by the parcels is the same (see Fig. 8). It follows that $|\Delta T| = T_0 - T_{\text{min}}$ increases monotonically with r_0 . For temperature-limit events, N_i increases exponentially with $|\Delta T|$ (recall Fig. 5 and Eq. 20), and so it must increase exponentially with r_0 . As r_0 increases, N_i increases until reaching a limit above which the nucleation event must be vapour-limit (see e.g. Fig. 5). Thus, for a given temperature time series, r_0 controls N_i and also determines whether the nucleation event is temperature- or vapour-limit.

For example, consider a temperature time series defined by a minimum of $T_{\text{min}} = 194.7$ K, a cooling rate associated with $w = +0.02 \text{ ms}^{-1}$ before T_{min} is reached, and a warming rate associated with $w = -0.02 \text{ ms}^{-1}$ after T_{min} is reached (see Fig. 8). This temperature time series is similar to the profiles we have studied earlier in Sect. 4.2. Consider three air parcels following this temperature time series, but for which $r_0 = \{1.77; 1.79; 1.81\} \times 10^{-5} \text{ kg kg}^{-1}$. All three air parcels experience nucleation, and in all cases $T_{\text{min}} = 194.7$ K occurs during the nucleation periods. However, our calculations give $T_0 = \{194.9; 195.0; 195.1\}$ K and $N_i = \{4.8 \times 10^{-1}; 8.4 \times 10^1; 3.6 \times 10^3\} \text{ L}^{-1}$ respectively for the three parcels. Moreover, the two drier air parcels experience temperature-limit nucleation events, whereas the moist air parcel experiences a vapour-limit event. As illustrated here, small differences in r_0 result in many orders of magnitude changes

8786

in N_i . Such a strong dependence of N_i on r_0 could explain the large-amplitude, small-scale heterogeneities in the INC as observed in cirrus clouds by Jensen et al. (2013).

6 Conclusions

We have simulated homogeneous ice nucleation using temperature time series data collected at high frequency by long-duration balloon flights near the tropical tropopause. The simulated nucleation events can be conceptually categorised as either vapour-limit or temperature-limit. For vapour-limit events, nucleation is limited by the depletion of water vapour. In contrast, for temperature-limit events, nucleation is controlled by the fluctuations in temperature (while the depletion in water vapour is negligible). The INC obtained for temperature-limit events is smaller than that obtained for vapour-limit events.

Our calculations of temperature-limit events confirm the finding by Spichtinger and Krämer (2013) that high-frequency fluctuations in temperature may limit the INC obtained by homogeneous freezing. Indeed, small INC is obtained if the gravity waves produce large but non-persistent cooling rates such that the absolute drop in temperature (i.e. the difference between the temperature at the threshold of nucleation and the minimum temperature obtained during nucleation) remains small. This relationship between the INC and temperature has been illustrated here both empirically and analytically.

In addition to the fluctuations in temperature, small variations in the initial water vapour content of the air parcels can also lead to large variations in the INC obtained by nucleation. Moreover, post-nucleation processes acting during the cirrus life cycle contribute to modify the cloud original characteristics. Simulations of cirrus clouds in the TTL by Dinh et al. (2012, 2014) show that the INC decreases by several orders of magnitude as the cloud ages. For these reasons, we suggest that homogeneous ice nucleation (even acting alone in the absence of heterogeneous freezing) is not incon-

8787

sistent with recent observations of cirrus clouds in the TTL, that indicate generally low but highly variable INC (Jensen et al., 2013).

Finally, it is encouraging that the INC for temperature-limit events does not depend on the deposition coefficient, a parameter still poorly constrained by theoretical understanding as well as laboratory measurements and field observations.

Acknowledgements. The data used for simulations in this work was collected during the project “Concordiasi,” which is supported by the following agencies: Météo-France, CNES, CNRS/INSU, NSF, NCAR, University of Wyoming, Purdue University, University of Colorado, Alfred Wegener Institute, Met Office, and ECMWF. Concordiasi also benefited from the logistic and financial support of the Institut polaire français Paul Emile Victor (IPEV), Programma Nazionale di Ricerche in Antartide (PNRA), United States Antarctic Program (USAP), British Antarctic Survey (BAS), and from measurements by the Baseline Surface Radiation Network (BSRN) at Concordia.

Tra Dinh acknowledges support from the NOAA Climate and Global Change Postdoctoral Fellowship Program, and NSF grant AGS-1417659. This collaborative research emerged from Tra Dinh’s visit to the Laboratoire de Météorologie Dynamique, which was supported by the “Tropical Cirrus” project of École Polytechnique’s “Chaire pour le Développement Durable.” Aurélien Podglajen, Albert Hertzog, Bernard Legras and Riwal Plougonven received support from the ANR project “Stradyvarius” (ANR-13-BS06-0011-01).

References

- Barahona, D. and Nenes, A.: Parameterization of cirrus cloud formation in large-scale models: homogeneous nucleation, *J. Geophys. Res.*, 113, D11211, doi:10.1029/2007JD009355, 2008. 8773
- Boccaro, G., Hertzog, A., Vincent, R. A., and Vial, F.: Estimation of gravity-wave momentum fluxes and phase speeds from quasi-Lagrangian stratospheric balloon flights. Part I: Theory and simulations, *J. Atmos. Sci.*, 65, 3042–3055, doi:10.1175/2008JAS2709.1, 2008. 8774, 8775

8788

- Brewer, A. W.: Evidence for a world circulation provided by the measurements of helium and water vapour distribution in the stratosphere, *Q. J. Roy. Meteor. Soc.*, 75, 351–363, doi:10.1002/qj.49707532603, 1949. 8772
- Chen, Y., Kreidenweis, S. M., McInnes, L. M., Rogers, D. C., and DeMott, P. J.: Single particle analyses of ice nucleating aerosols in the upper troposphere and lower stratosphere, *Geophys. Res. Lett.*, 25, 1391–1394, doi:10.1029/97GL03261, 1998. 8773, 8776
- 5 Corti, T., Luo, B. P., Fu, Q., Vömel, H., and Peter, T.: The impact of cirrus clouds on tropical troposphere-to-stratosphere transport, *Atmos. Chem. Phys.*, 6, 2539–2547, doi:10.5194/acp-6-2539-2006, 2006. 8772
- 10 Davis, S., Hlavka, D., Jensen, E., Rosenlof, K., Yang, Q., Schmidt, S., Borrmann, S., Frey, W., Lawson, P., Voemel, H., and Bui, T. P.: In situ and lidar observations of tropopause subvisible cirrus clouds during TC4, *J. Geophys. Res.*, 115, D00J17, doi:10.1029/2009JD013093, 2010. 8773
- Dinh, T. and Durran, D. R.: A hybrid bin scheme to solve the condensation/evaporation equation using a cubic distribution function, *Atmos. Chem. Phys.*, 12, 1003–1011, doi:10.5194/acp-12-1003-2012, 2012. 8776
- 15 Dinh, T. and Fueglistaler, S.: Cirrus, transport, and mixing in the tropical upper troposphere, *J. Atmos. Sci.*, 71, 1339–1352, doi:10.1175/JAS-D-13-0147.1, 2014a. 8772
- Dinh, T. and Fueglistaler, S.: Microphysical, radiative and dynamical impacts of thin cirrus clouds on humidity in the tropical tropopause layer and stratosphere, *Geophys. Res. Lett.*, 20, 41, 6949–6955, doi:10.1002/2014GL061289, 2014b. 8772
- Dinh, T., Durran, D. R., and Ackerman, T.: Cirrus and water vapor transport in the tropical tropopause layer – Part 1: A specific case modeling study, *Atmos. Chem. Phys.*, 12, 9799–9815, doi:10.5194/acp-12-9799-2012, 2012. 8787
- 25 Dinh, T., Fueglistaler, S., Durran, D., and Ackerman, T.: Cirrus and water vapour transport in the tropical tropopause layer – Part 2: Roles of ice nucleation and sedimentation, cloud dynamics, and moisture conditions, *Atmos. Chem. Phys.*, 14, 12225–12236, doi:10.5194/acp-14-12225-2014, 2014. 8787
- Fueglistaler, S., Dessler, A. E., Dunkerton, T. J., Folkins, I., Fu, Q., and Mote, P. W.: Tropical tropopause layer, *Rev. Geophys.*, 47, RG1004, doi:10.1029/2008RG000267, 2009. 8772
- 30 Jensen, E. J., Toon, O. B., Pfister, L., and Selkirk, H. B.: Dehydration of the upper troposphere and lower stratosphere by subvisible cirrus clouds near the tropical tropopause, *Geophys. Res. Lett.*, 23, 825–828, doi:10.1029/96GL00722, 1996. 8772

8789

- Jensen, E. J., Pfister, L., Bui, T.-P., Lawson, P., and Baumgardner, D.: Ice nucleation and cloud microphysical properties in tropical tropopause layer cirrus, *Atmos. Chem. Phys.*, 10, 1369–1384, doi:10.5194/acp-10-1369-2010, 2010. 8773
- 5 Jensen, E. J., Pfister, L., and Bui, T. P.: Physical processes controlling ice concentrations in cold cirrus near the tropical tropopause, *J. Geophys. Res.*, 117, D11205, doi:10.1029/2011JD017319, 2012. 8773
- Jensen, E. J., Diskin, G., Lawson, R. P., Lance, S., Bui, T. P., Hlavka, D., McGill, M., Pfister, L., Toon, O. B., and Gao, R.: Ice nucleation and dehydration in the Tropical Tropopause Layer, *P. Natl. Acad. Sci. USA*, 110, 2041–2046, doi:10.1073/pnas.1217104110, 2013. 8787, 8788
- 10 Kärcher, B. and Lohmann, U.: A parameterization of cirrus cloud formation: Homogeneous freezing of supercooled aerosols, *J. Geophys. Res.*, 107, AAC4.1–AAC4.10, doi:10.1029/2001JD000470, 2002. 8777
- Kärcher, B., Dörnbrack, A., and Sölch, I.: Supersaturation variability and cirrus ice crystal size distributions, *J. Atmos. Sci.*, 71, 2905–2926, doi:10.1175/JAS-D-13-0404.1, 2014. 8772
- 15 Koop, T., Luo, B., Tsias, A., and Peter, T.: Water activity as the determinant for homogeneous ice nucleation in aqueous solutions, *Nature*, 406, 611–614, doi:10.1038/35020537, 2000. 8776, 8777, 8782, 8783
- Krämer, M., Schiller, C., Afchine, A., Bauer, R., Gensch, I., Mangold, A., Schlicht, S., Spelten, N., Sitnikov, N., Borrmann, S., de Reus, M., and Spichtinger, P.: Ice supersaturations and cirrus cloud crystal numbers, *Atmos. Chem. Phys.*, 9, 3505–3522, doi:10.5194/acp-9-3505-2009, 2009. 8773, 8778
- 20 Lawson, R. P., Pilon, B., Baker, B., Mo, Q., Jensen, E., Pfister, L., and Bui, P.: Aircraft measurements of microphysical properties of subvisible cirrus in the tropical tropopause layer, *Atmos. Chem. Phys.*, 8, 1609–1620, doi:10.5194/acp-8-1609-2008, 2008. 8773
- 25 Lohmann, U. and Roeckner, E.: Influence of cirrus cloud radiative forcing on climate and climate sensitivity in a general circulation model, *J. Geophys. Res.*, 100, 16305, doi:10.1029/95JD01383, 1995. 8772
- Magee, N., Moyle, A. M., and Lamb, D.: Experimental determination of the deposition coefficient of small cirrus-like ice crystals near -50° Celsius, *Geophys. Res. Lett.*, 33, L17813, doi:10.1029/2006GL026665, 2006. 8776
- 30 Massman, W. J.: On the nature of vertical oscillations of constant volume balloons, *J. Appl. Meteorol.*, 17, 1351–1356, doi:10.1175/1520-0450(1978)017<1351:OTNOVO>2.0.CO;2, 1978. 8774

8790

- Nastrom, G. D.: The response of superpressure balloons to gravity waves, *J. Appl. Meteorol.*, 19, 1013–1019, doi:10.1175/1520-0450(1980)019<1013:TROSBT>2.0.CO;2, 1980. 8774
- Podglajen, A., Hertzog, A., Plougonven, R., and Žagar, N.: Assessment of the accuracy of (re)analyses in the equatorial lower stratosphere, *J. Geophys. Res.*, 119, 11166–11188, doi:10.1002/2014JD021849, 2014. 8774
- Pruppacher, H. R. and Klett, J. D.: *Microphysics of clouds and precipitation*, D. Reidel Publishing Company, Dordrecht, Holland, 1978. 8776
- Rabier, F., Bouchard, A., Brun, E., Doerenbecher, A., Guedj, S., Guidard, V., Karbou, F., Peuch, V.-H., Amraoui, L. E., Puech, D., Genthon, C., Picard, G., Town, M., Hertzog, A., Vial, F., Cocquerez, P., Cohn, S. A., Hock, T., Fox, J., Cole, H., Parsons, D., Powers, J., Romberg, K., VanAndel, J., Deshler, T., Mercer, J., Haase, J. S., Avallone, L., Kalnajs, L., and Mechoso, C. R.: The Concordiasi project in Antarctica, *B. Am. Meteorol. Soc.*, 91, 69–86, doi:10.1175/2009bams2764.1, 2010. 8774
- Ren, C. and Mackenzie, A. R.: Cirrus parametrization and the role of ice nuclei, *Q. J. Roy. Meteor. Soc.*, 131, 1585–1605, doi:10.1256/qj.04.126, 2005. 8777
- Rogers, D. C., Demott, P. J., Kreidenweis, S. M., and Chen, Y.: Measurements of ice nucleating aerosols during SUCCESS, *Geophys. Res. Lett.*, 25, 1383–1386, doi:10.1029/97GL03478, 1998. 8773
- Skrotzki, J., Connolly, P., Schnaiter, M., Saathoff, H., Möhler, O., Wagner, R., Niemand, M., Ebert, V., and Leisner, T.: The accommodation coefficient of water molecules on ice – cirrus cloud studies at the AIDA simulation chamber, *Atmos. Chem. Phys.*, 13, 4451–4466, doi:10.5194/acp-13-4451-2013, 2013. 8776
- Spichtinger, P. and Krämer, M.: Tropical tropopause ice clouds: a dynamic approach to the mystery of low crystal numbers, *Atmos. Chem. Phys.*, 13, 9801–9818, doi:10.5194/acp-13-9801-2013, 2013. 8773, 8779, 8787
- Vincent, R. A. and Hertzog, A.: The response of superpressure balloons to gravity wave motions, *Atmos. Meas. Tech.*, 7, 1043–1055, doi:10.5194/amt-7-1043-2014, 2014. 8774

8791

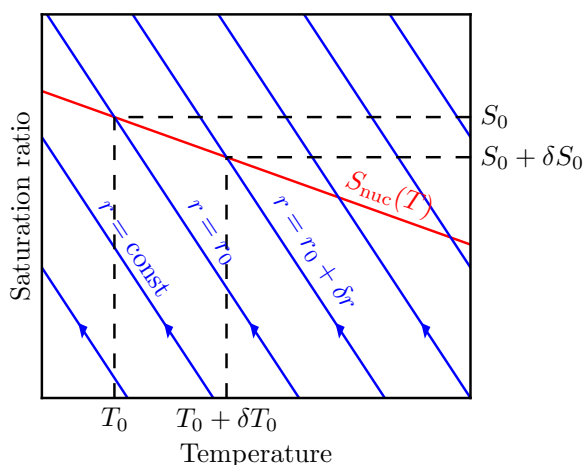


Figure 1. Diagram illustrating the initial conditions of the air parcels. Prior to nucleation air parcels follow isolines of water vapour mixing ratio r (shown here in blue) and approach the curve $S_{\text{nuc}}(T)$ from below (as indicated by the arrows). Nucleation begins at the intersections of the r isolines with the curve $S_{\text{nuc}}(T)$.

8792

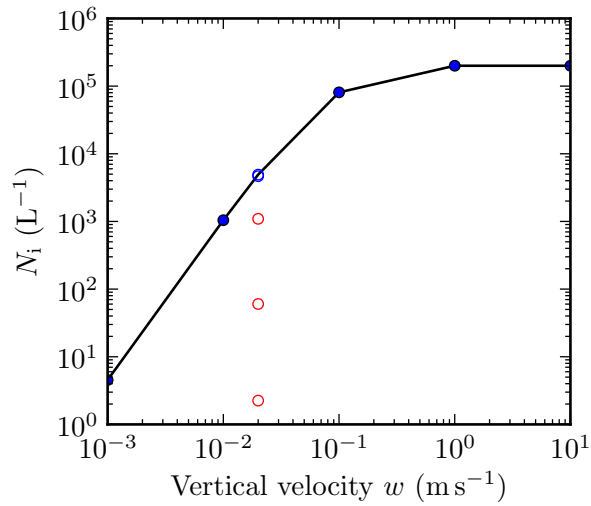


Figure 2. Number of ice crystals obtained for the five nucleation events forced by constant $w = \{0.001; 0.01; 0.1; 1; 10\} \text{ m s}^{-1}$ (solid circles), and the five nucleation events forced by $w = \pm 0.02 \text{ m s}^{-1}$, see Eq. (7) (open circles). Vapour-limit events (blue circles) are obtained with constant w , or with $w = \pm 0.02 \text{ m s}^{-1}$ and $t_s = \{32; 36\} \text{ min}$. Temperature-limit events (red circles) are obtained with $w = \pm 0.02 \text{ m s}^{-1}$ and $t_s = \{20; 24; 28\} \text{ min}$. The INCs are almost the same for the two vapour-limit events obtained with $w = \pm 0.02 \text{ m s}^{-1}$, hence the two open blue circles overlap.

8793

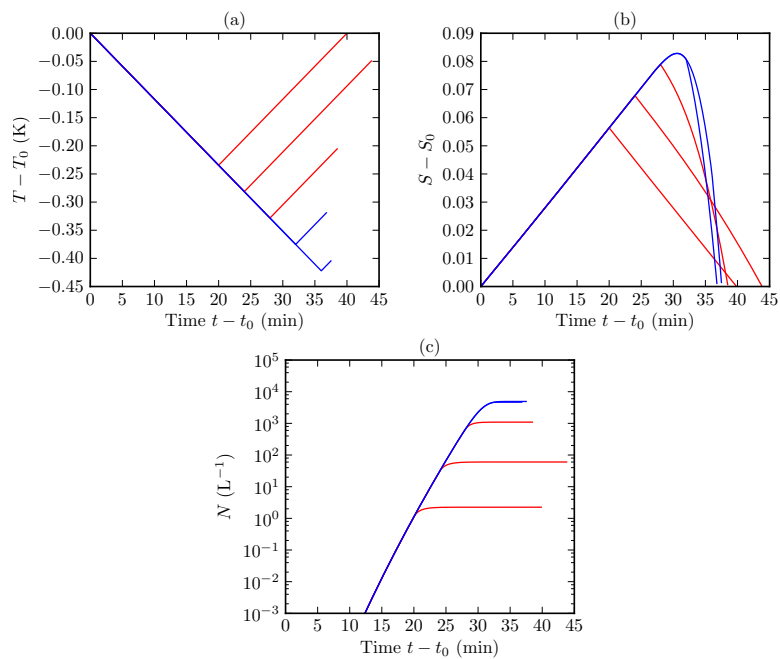


Figure 3. Evolution of temperature, saturation ratio and INC during the five nucleation events forced by $w = \pm 0.02 \text{ m s}^{-1}$ as defined by Eq. (7). Blue curves show vapour-limit events and red curves show temperature-limit events.

8794

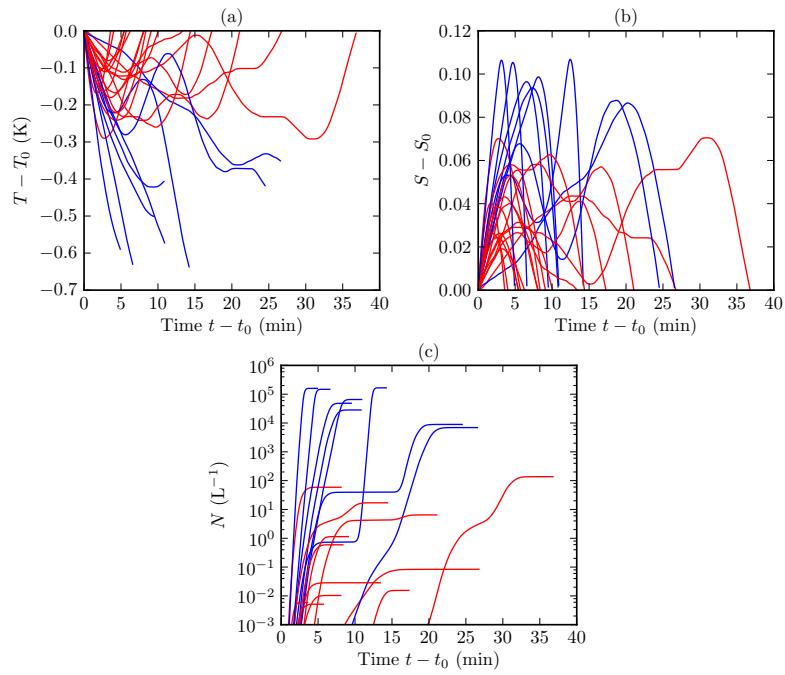


Figure 4. Same as Fig. 3 but for nucleation events forced by the temperature perturbations taken from the balloon data.

8795

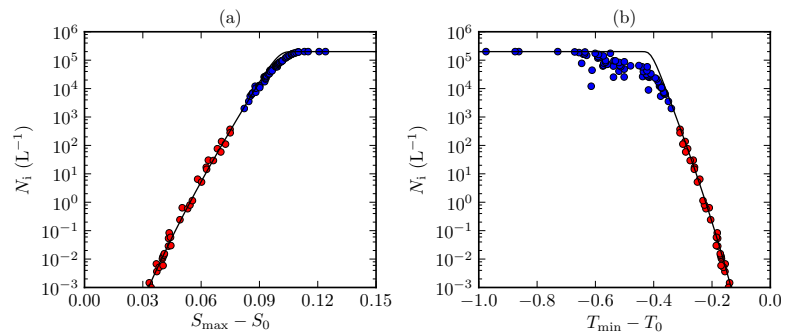


Figure 5. Number of ice crystals nucleated at $T_0 = 195$ K with the balloon temperature perturbation time series. Blue circles show vapour-limit nucleation events. Red circles show temperature-limit nucleation events. The solid curve is obtained from Eqs. (16)–(20) with $\mu = 0.02 \text{ s}^{-1}$.

8796

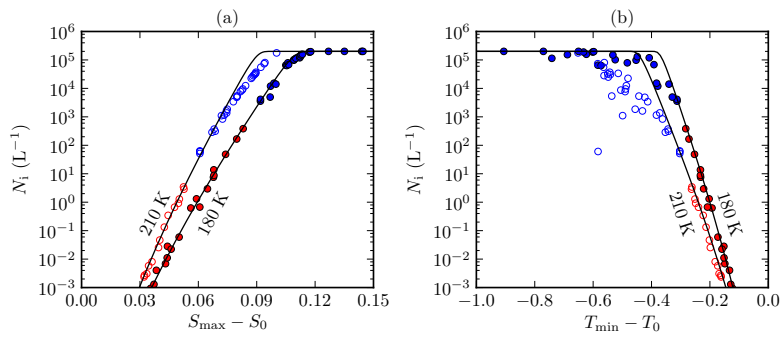


Figure 6. Same as Fig. 5 but for $T_0 = 180$ K (solid circles) and 210 K (empty circles).

8797

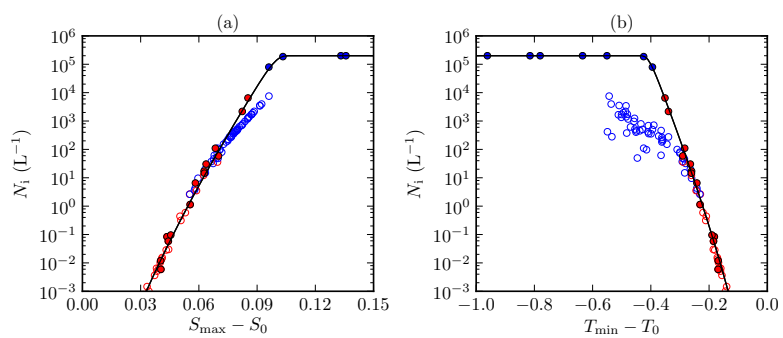


Figure 7. Same as Fig. 5 but for $\alpha = 0.001$ (solid circles) and $\alpha = 1$ (empty circles).

8798

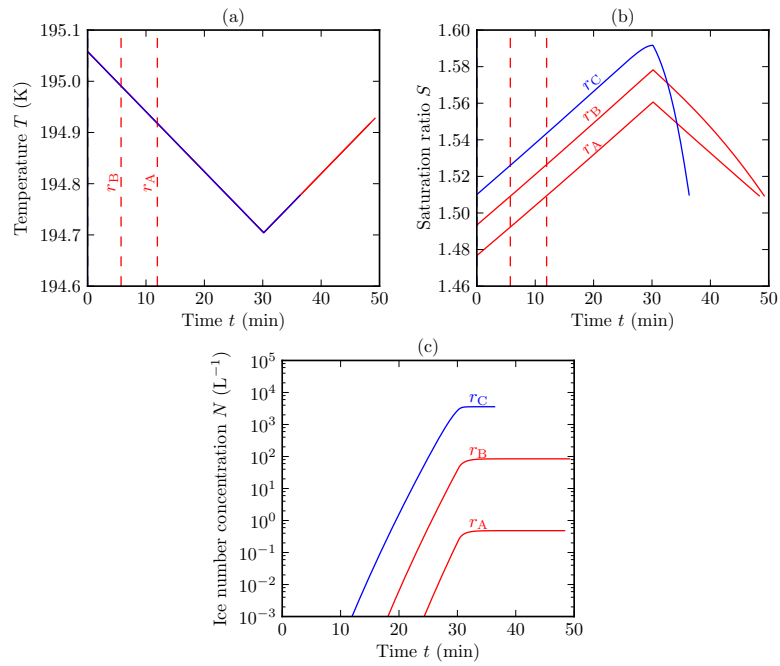


Figure 8. Evolution of temperature, saturation ratio and INC for three air parcels with slightly different initial water vapour mixing ratios: $\{r_A = 1.77; r_B = 1.79; r_C = 1.81\} \times 10^{-5} \text{ kg kg}^{-1}$. The three parcels follow the same temperature time series as shown in (a), but the differences in their initial water vapour contents result in widely different INCs. The two dry parcels experience temperature-limit (red) events, which begin at the times indicated by the dash lines in (a) and (b). The moist parcel experiences a vapour-limit (blue) event, which starts from $t = 0$.